Journal of Materials Chemistry

Dynamic Article Links

Cite this: *J. Mater. Chem.*, 2011, **21**, 10489

www.rsc.org/materials

PAPER

$(Ca,Mg,Sr)_9Y(PO_4)_7:Eu^{2+},Mn^{2+}$: Phosphors for white-light near-UV LEDs through crystal field tuning and energy transfer

Chien-Hao Huang,[a] Pin-Jiun Wu,[b] Jyh-Fu Lee[b] and Teng-Ming Chen*[a]

Received 9th March 2011, Accepted 27th April 2011
DOI: 10.1039/c1jm11018g

Two series of single-composition $(Ca,Mg,Sr)_9Y(PO_4)_7:Eu^{2+}$ and $(Ca_{0.5}Sr_{0.5})_9Y(PO_4)_7:Eu^{2+},Mn^{2+}$ phosphors were synthesized *via* high-temperature solid-state reactions. Their emission colors could be tuned from blue to green and eventually to red through tuning the crystal field splitting and energy transfer. On examining the Mn^{2+} concentration-dependent photoluminescence properties, we found that co-doping with Mn^{2+} would lead to a change in Eu^{2+}/Eu^{3+} ratio. Moreover, an energy transfer from Eu^{2+} to Mn^{2+} occurs because of the spectral overlap between the emission band of Eu^{2+} and the excitation band of Mn^{2+}. The resonance-type energy transfer *via* a dipole–quadrupole interaction mechanism was supported by decay lifetime data and the critical distance of energy transfer was calculated to be 11.09 Å. A trichromatic white-light emitting diode was fabricated by integrating a 380 nm near-ultraviolet (n-UV) chip comprising yellow-emitting $(Ca_{0.5}Sr_{0.5})_9Y(PO_4)_7:0.007Eu^{2+},0.02Mn^{2+}$ and blue-emitting $(Ca_{0.5}Mg_{0.5})_9Y(PO_4)_7:0.007Eu^{2+}$ phosphors into a single package. Such a composite device emitted white light with a correlated color temperature of 6303 K, a color rendering index of 87.4, and color coordinates (0.314, 0.348) close to those of ideal white light. The results suggest that a phosphor blend of $(Ca_{0.5}Sr_{0.5})_9Y(PO_4)_7:0.007Eu^{2+},0.02Mn^{2+}$ and $(Ca_{0.5}Mg_{0.5})_9Y(PO_4)_7:0.007Eu^{2+}$ is potentially useful for white n-UV light-emitting diodes (LEDs).

1 Introduction

In recent years, it was shown that white light-emitting diodes (white LEDs) can be generated by combining a blue-emitting InGaN LED chip and a yellow-emitting garnet phosphor $Y_3Al_5O_{12}:Ce^{3+}$ (YAG:Ce^{3+}).[1,2] However, the major disadvantage of such a combination is a low color rendering index (CRI, *Ra*)[3] due to the lack of red-light contribution[4,5] and a high correlated color temperature. To improve the CRI of white-LEDs, trichromatic white-LEDs are considered to be potentially useful because of their high color rendering properties. Chiu *et al.*[6] demonstrated that a near-ultraviolet (n-UV) LED chip consisting of three different phases, red- ($CaAlSiN_3:Eu^{2+}$), green- ($(Ba,Sr)_2SiO_4:Eu^{2+}$), and blue-emitting ($Ca_2PO_4Cl:Eu^{2+}$) phosphors, gave a relatively high *Ra* of 93.4. Guo *et al.*[7] reported that single-phase full-color-emitting $Ba_2Ca(BO_3)_2:Ce^{3+},Mn^{2+}$ phosphors pumped by UV-LEDs exhibit three broadband emissions centered at 420 (blue), 480 (green), and 625 nm (red) with the *Ra* value being 55–95. Lee *et al.*[8] described white-LEDs using $Ba_3MgSi_2O_8:Eu^{2+},Mn^{2+}$ commodity phosphors—a blend of $CaMgSi_2O_6:Eu^{2+},Mn^{2+}$ and $(Ba,Sr)_2SiO_4:Eu^{2+}$ phosphors pumped with a 365 UV-LED chip. Their results showed a *Ra* value of 71–88.

In this article, we report an unprecedented phosphor whose emission color is tunable from blue through green to red. We have systematically investigated the influence of crystal field splitting of Mg^{2+}, Ca^{2+}, and Sr^{2+} ions on emission wavelength in the $Ca_9Y(PO_4)_7:Eu^{2+}$ structure. Besides, energy transfer between Eu^{2+} and Mn^{2+} ions in the $(Ca_{0.5}Sr_{0.5})_9Y(PO_4)_7:Eu^{2+},Mn^{2+}$ phosphors was confirmed both experimentally and theoretically by calculating the critical energy transfer distance between these ions. Finally, we succeeded to fabricate white n-UV LEDs and thoroughly examined their optical properties.

2 Experimental

2.1 Materials and synthesis

Three series of polycrystalline phosphors with the compositions of $(Ca_{1-x}Mg_x)_9Y(PO_4)_7:Eu^{2+}$ (CMYP:Eu^{2+}), $(Ca_{1-y}Sr_y)_9Y(PO_4)_7:Eu^{2+}$ (CSYP:Eu^{2+}), and $(Ca_{0.5}Sr_{0.5})_9Y(PO_4)_7:Eu^{2+},Mn^{2+}$ (CSYP:Eu^{2+},Mn^{2+}) were synthesized *via* high-temperature solid-state reactions. A stoichiometric mixture of $CaCO_3$ (A. R., 99.9%), MgO (A. R., 99%), $SrCO_3$ (A. R., 99.9%), Y_2O_3 (A. R., 99.99%), $(NH_4)_2HPO_4$ (Merck, ≥99%), Eu_2O_3 (A. R., 99.99%), MnO (A. R., 99.9%) were thoroughly mixed, ground in an agate mortar, transferred to an alumina boat, and calcined under a reducing atmosphere (15% H_2/85% N_2) at 1000–1400 °C for 8 h.

[a]*Phosphors Research Laboratory and Department of Applied Chemistry, National Chiao Tung University, Hsinchu, 30010, Taiwan. E-mail: tmchen@mail.nctu.edu.tw; Tel: +886-35731695*
[b]*National Synchrotron Radiation Research Center, Hsinchu, 30076, Taiwan R.O.C.*

2.2 Materials characterization

Powder X-ray diffraction (XRD) data over the angular range $10° \leqq 2\theta \leqq 80°$ were obtained using Cu-Kα radiation (Bruker AXS D8), operating at 40 kV and 40 mA. X-ray photoelectron spectroscopy (XPS) measurements were carried out with Kratos Axis Ultra DLD, employing MCP stack & delay-line photoelectron detector with scanned & snapshot spectroscopy modes. A Mg/Al achromatic X-ray source with maximum power of 450 W was used along with a 500 mm Rowland circle Al monochromator. The photoluminescence (PL) and photoluminescence excitation (PLE) spectra were measured using a Spex Fluorolog-3 Spectrofluorometer equipped with a 450 W Xe light source. White-light LED lamps were fabricated by integrating a mixture of transparent silicon resin and phosphors blend of $(Ca_{0.5}Sr_{0.5})_9Y(PO_4)_7$:0.007$Eu^{2+}$,0.02$Mn^{2+}$ and $(Ca_{0.5}Mg_{0.5})_9Y(PO_4)_7$:0.007$Eu^{2+}$ on a commodity n-UV LED chip (AOT, Taiwan, Product No: C06HC, Spec: 380V06, wavelength peak: 375–380 nm, chip size: 40 × 40 mil, forward voltage: 3.8–4.0 V, power: 50–60 mW). The Commission International de I'Eclairage (CIE) chromaticity coordinates for all samples were measured by a Laiko DT-101 color analyzer equipped with a CCD detector (Laiko Co., Tokyo, Japan). XANES spectra at the Eu L_3-edge were recorded at a wiggler beamline BL17C of the National Synchrotron Radiation Research Center (NSRRC). Lytle detector was used to measure the X-ray fluorescence intensities from powdered samples at room temperature. The threshold energy was determined from a pure Eu_2O_3 reference compound. For the analysis of XANES data, standard procedures were followed, including pre-edge and post-edge background subtraction and normalization with respect to the edge jump.

3 Results and discussion

3.1 Crystal structure

Fig. 1 shows the powder XRD patterns for representative CYP:Eu^{2+}, CMYP:Eu^{2+}, CSYP:Eu^{2+}, and CSYP:Eu^{2+},Mn^{2+} phosphors, along with the reference diffraction lines based on JCPDS file no. 046-0402.[9] It was found that as Ca^{2+} is substituted by the smaller Mg^{2+} ion, the entire diffraction profile shifts slightly towards a higher 2θ angle. On the other hand, if Ca^{2+} is substituted by the larger Sr^{2+} ion, the diffraction profile shifts towards a lower 2θ angle. The impurity phase will appear for the host doped with higher concentrations of Mg^{2+} or Sr^{2+} ions (*e.g.* > 0.5 mol%). Since there are no extra peaks observed in the XRD patterns for CMYP:Eu^{2+} and CSYP:Eu^{2+} phosphors, even for the Eu^{2+}/Mn^{2+} co-doped CMYP and CSYP samples, the results indicate that the phosphors retain a single-phase structure. The crystal structure of $Ca_9Y(PO_4)_7$ is rhombohedral, space group *R*3*c* (No.161), with lattice parameters of $a = 10.4442$ Å, $c = 37.324$ Å, $V = 3525.89$ Å,[3] and $Z = 6$. The near neighbors of the Ca^{2+} cation include two eight-fold Ca(1), Ca(2) and one nine-fold coordinated Ca(3) surrounded by oxygen atoms. Therefore, based on the effective ionic radii and charge balance of cations with different coordination numbers, we proposed that Mg^{2+}, Sr^{2+}, Eu^{2+} and Mn^{2+} should randomly occupy the three Ca^{2+} sites in the host structure.

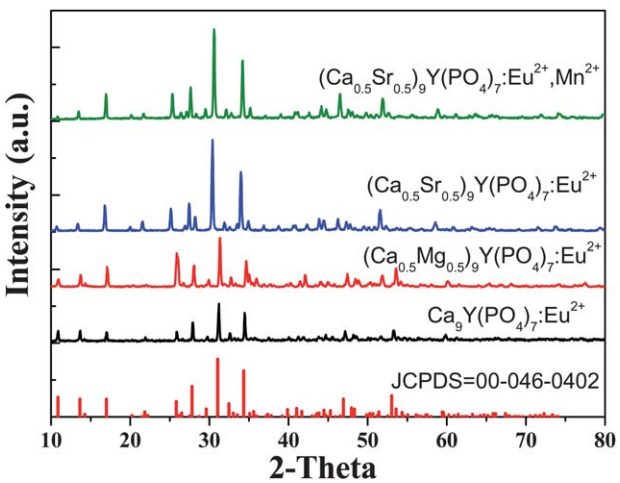

Fig. 1 Powder XRD patterns for $Ca_9Y(PO_4)_7$:Eu^{2+}, $(Ca_{0.5}Mg_{0.5})_9Y(PO_4)_7$:$Eu^{2+}$, $(Ca_{0.5}Sr_{0.5})_9Y(PO_4)_7$:$Eu^{2+}$, $(Ca_{0.5}Sr_{0.5})_9Y(PO_4)_7$:$Eu^{2+}$,$Mn^{2+}$ phosphors.

3.2 Photoluminescence properties

X-ray photoelectron spectroscopy (XPS) allows us to access the elemental identification of all tested samples. Photoelectron survey spectra of the pristine $(Ca_{0.5}Sr_{0.5})_9Y(PO_4)_7$ and $(Ca_{0.473}Eu_{0.007}Mn_{0.02}Sr_{0.5})_9Y(PO_4)_7$ powdered samples are plotted in Fig. 2, revealing almost the same features with the binding energy below 600 eV. The doped elements, Eu and Mn, were detected in the $(Ca_{0.473}Eu_{0.007}Mn_{0.02}Sr_{0.5})_9Y(PO_4)_7$. The Eu $3d_{3/2}$, $3d_{5/2}$ and the Mn $2p_{1/2}$, $2p_{3/2}$ core-level peaks are located at the binding energies around 1163, 1133 and 648, 638 eV, respectively, exhibiting weak intensities due to low doping concentration.

Fig. 3 illustrates the emission spectra of $(Ca_{0.993-x}Mg_x)_9Y(PO_4)_7$:0.007$Eu^{2+}$ and $(Ca_{0.993-y}Sr_y)_9Y(PO_4)_7$:0.007 Eu^{2+}, with x and y corresponding to various molar concentrations (0–0.5 mol %) of Mg^{2+} and Sr^{2+}, respectively, under 380 nm excitation. As indicated in Fig. 3, there is a continuous blue-shift in the emission wavelength from 486 to 435 nm with increasing Mg^{2+} content ($x \leqq 0.5$) and a red-shift from 486 to 508 nm with increasing Sr^{2+} concentration ($y \leqq 0.5$). The chromaticity coordinates for $(Ca_{0.993-x}Mg_x)_9Y(PO_4)_7$:0.007$Eu^{2+}$ and $(Ca_{0.993-y}Sr_y)_9Y(PO_4)_7$:0.007$Eu^{2+}$ phosphors respectively range from (0.179, 0.301) to (0.162, 0.098) and from (0.179, 0.301) to (0.273, 0.459). These results indicate that the hue or emission color is tunable from blue to blue-greenish and to green in the visible region of the spectrum by varying the divalent metal ions,[10] such as: Mg^{2+} or Sr^{2+}, as summarized in Table 1. According to reports by Robertson *et al.*[11] and Jang *et al.*,[12] crystal field splitting (*Dq*) can be determined by the following equation:[13]

$$D\,q = \frac{1}{6} Ze^2 \frac{r^4}{R^5} \quad (1)$$

where *Dq* is a measure of the energy level separation, *Z* is the anion charge, *e* is the electron charge, *r* is the radius of the *d* wavefunction, and *R* is the bond length. When Ca^{2+} is substituted by a smaller Mg^{2+} ion, the distance between Eu^{2+} and O^{2-} becomes longer and the magnitude of the crystal field

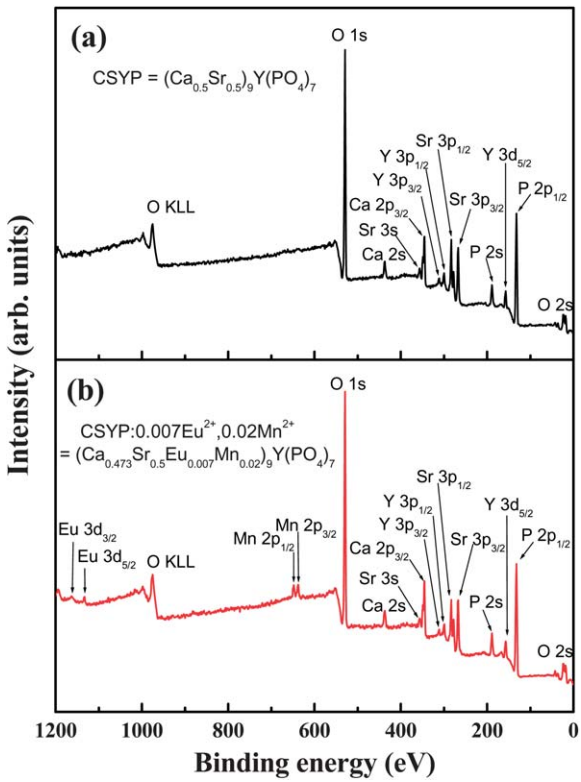

Fig. 2 XPS survey spectra of (a) $(Ca_{0.5}Sr_{0.5})_9Y(PO_4)_7$ and (b) $(Ca_{0.473}Eu_{0.007}Mn_{0.02}Sr_{0.5})_9Y(PO_4)_7$.

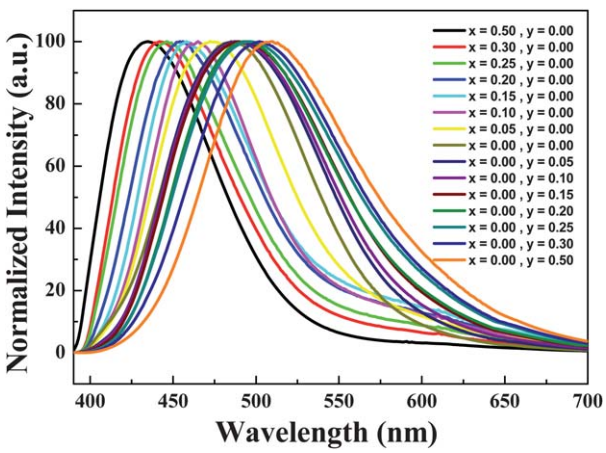

Fig. 3 Dependence of emission spectra of $(Ca_{0.993-x-y}Mg_xSr_y)_9Y(PO_4)_7$:0.007$Eu^{2+}$ phosphors on concentrations of Mg^{2+} and Sr^{2+}.

decreases, so that there is a continuous increase in the blue-shift with the doped Mg^{2+} concentration. In contrast, when Ca^{2+} is substituted with a larger Sr^{2+} ion, the distance between Eu^{2+} and O^{2-} becomes shorter, which in turn increases the magnitude or strength of the crystal field. As a result, the 5*d* band of Eu^{2+} is lowered, and the emission wavelength is red-shifted from 486 to 508 nm as the doped Sr^{2+} content increases. The schematic diagram for crystal-field splitting of Eu^{2+} 5d energy level is shown in Fig. 4.[14]

The spectral overlap between the emission band of Eu^{2+} and the excitation band of Mn^{2+} was clearly observed in Fig. 5a. The

Table 1 Comparison of CIE chromaticity coordinates and optimal emission sites for $(Ca_{0.993-x-y}Mg_xSr_y)_9Y(PO_4)_7$:0.007$Eu^{2+}$ phosphors excited at 380 nm

Sample	Emission site	CIE (*x*, *y*)
$x = 0.50$, $y = 0.00$	435 nm	(0.162, 0.098)
$x = 0.30$, $y = 0.00$	442 nm	(0.175, 0.134)
$x = 0.25$, $y = 0.00$	446 nm	(0.181, 0.154)
$x = 0.20$, $y = 0.00$	454 nm	(0.193, 0.189)
$x = 0.15$, $y = 0.00$	458 nm	(0.192, 0.200)
$x = 0.10$, $y = 0.00$	465 nm	(0.191, 0.210)
$x = 0.05$, $y = 0.00$	472 nm	(0.186, 0.250)
$x = 0.00$, $y = 0.00$	486 nm	(0.179, 0.301)
$x = 0.00$, $y = 0.05$	487 nm	(0.195, 0.329)
$x = 0.00$, $y = 0.10$	489 nm	(0.204, 0.338)
$x = 0.00$, $y = 0.15$	492 nm	(0.217, 0.353)
$x = 0.00$, $y = 0.20$	494 nm	(0.223, 0.369)
$x = 0.00$, $y = 0.25$	496 nm	(0.238, 0.383)
$x = 0.00$, $y = 0.30$	502 nm	(0.249, 0.413)
$x = 0.00$, $y = 0.50$	508 nm	(0.273, 0.459)

photoluminescence (PL) spectrum of CSYP:Eu^{2+} shows a broad emission band from 400 to 700 nm with a strong green emission centered at 508 nm due to the $4f^65d^1 \rightarrow 4f^7$ ($^8S_{7/2}$) transition. There appear five excitation bands of CSYP:Mn^{2+} centered at 317, 343, 368, 408, and 469 nm, which can be assigned to the transitions from $^6A_1(^6S)$ to $^4T_1(^4P)$, $^4E(^4D)$, $^4T_2(^4D)$, [$^4A_1(^4G)$, $^4E(^4G)$], and $^4T_1(^4G)$, respectively.[15] The emission band centered at 632 nm corresponds to the spin-forbidden $^4T_1(^4G) \rightarrow {}^6A_1(^6S)$ transition of Mn^{2+}. Since these transitions are spin- and parity-forbidden, both the excitation and emission intensities are relatively weak due to the forbidden *d*–*d* transition of Mn^{2+}.[16] Energy transfer was expected to occur from Eu^{2+} to Mn^{2+} based on the significant spectral overlap observed, particularly between the emission band of CSYP:Eu^{2+} ($4f^65d^1 \rightarrow 4f^7$ transition) and the excitation band of CSYP:Mn^{2+} ($^6A_1(^6S) \rightarrow {}^4T_1(^4G)$ transition). Therefore, an effective resonance-type energy transfer from Eu^{2+} to Mn^{2+} was expected. Fig. 5b shows the emission spectra for Mn^{2+} at different values of *z* ($z = 0$–0.1) in CSYP:0.007Eu^{2+},*z*Mn^{2+} phosphors. The intensity of the Eu^{2+} emission at 508 nm decreases, and that of the Mn^{2+} emission at 632 nm increases, with increasing Mn^{2+} content until the Mn^{2+} content reached 0.07 mol%, at which point concentration quenching

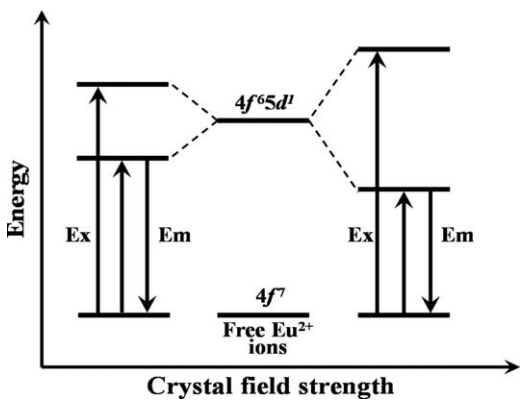

Fig. 4 Schematic diagram for Eu^{2+} 5d energy level in strong and weak crystal fields.

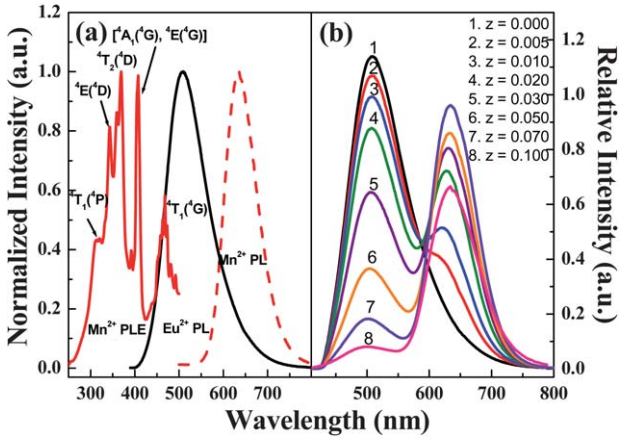

Fig. 5 (a) Spectral overlap between Eu^{2+} photoluminescence (PL) spectrum of CSYP:Eu^{2+} (black line) and PL excitation (PLE) spectrum of CSYP:Mn^{2+} (red line); (b) Emission spectra of Mn^{2+} at different values of z in CSYP:0.007Eu^{2+},zMn^{2+} phosphors excited at 380 nm.

started to occur. This phenomenon is attributable to the energy transfer from Eu^{2+} to Mn^{2+}.

Table 2 lists the CIE chromaticity coordinates with various Eu^{2+}/Mn^{2+} ratios in CSYP:0.007Eu^{2+},zMn^{2+} (z = 0–0.1) phosphors and their hues can be varied from green (0.273, 0.459) through yellow (0.358, 0.431) and eventually to red (0.565, 0.360).

Fig. 6a displays the normalized Eu L_3-edge XANES spectra of a series of CSYP:0.007Eu^{2+},zMn^{2+} phosphors. All spectra reveal two absorption features at 6972 and 6980 eV in the white-line region, which are attributed to $2p_{3/2} \rightarrow$ 5d electron transition in Eu^{2+} and Eu^{3+}, respectively.[17] As the concentration of doped Mn ions is increased, an increase in the peak intensity of Eu^{2+} and a reduction in that of Eu^{3+} can be observed. This observation represents the variation in the relative amount of Eu^{2+} and Eu^{3+} ions with doping Mn^{2+} ions.[18] Suppression of the oxidation of Eu^{2+} by co-doping Mn^{2+} ions can be related to the deficiency stabilization in the host material and the formation energy of the doped atom–vacancy pair.[19] Fig. 6b represents the quantitative results of the Eu^{2+} fraction, as a function of Mn^{2+} concentration, obtained from the fitting of the XANES spectra shown in Fig. 6a using two sets of a Lorentzian (white lines) and an arctangent function (edge jump).[20] We found that the fraction of Eu^{2+} increases with increasing Mn^{2+} concentration, exhibiting a dramatic change for $z < 0.01$ and then a slow variation for $z > 0.01$. Since the luminescence intensities of Eu^{2+} change in an

Table 2 Comparison of CIE chromaticity coordinates for $(Ca_{0.493-z}Sr_{0.5})_9Y(PO_4)_7$:0.007$Eu^{2+}$,$zMn^{2+}$ phosphors excited at 380 nm

Sample compositions	CIE (x, y)
$(Ca_{0.493}Eu_{0.007}Mn_{0.000}Sr_{0.5})_9Y(PO_4)_7$	(0.273, 0.459)
$(Ca_{0.488}Eu_{0.007}Mn_{0.005}Sr_{0.5})_9Y(PO_4)_7$	(0.300, 0.451)
$(Ca_{0.483}Eu_{0.007}Mn_{0.010}Sr_{0.5})_9Y(PO_4)_7$	(0.321, 0.443)
$(Ca_{0.473}Eu_{0.007}Mn_{0.020}Sr_{0.5})_9Y(PO_4)_7$	(0.358, 0.431)
$(Ca_{0.463}Eu_{0.007}Mn_{0.030}Sr_{0.5})_9Y(PO_4)_7$	(0.396, 0.415)
$(Ca_{0.443}Eu_{0.007}Mn_{0.050}Sr_{0.5})_9Y(PO_4)_7$	(0.462, 0.389)
$(Ca_{0.423}Eu_{0.007}Mn_{0.070}Sr_{0.5})_9Y(PO_4)_7$	(0.542, 0.368)
$(Ca_{0.393}Eu_{0.007}Mn_{0.100}Sr_{0.5})_9Y(PO_4)_7$	(0.565, 0.360)

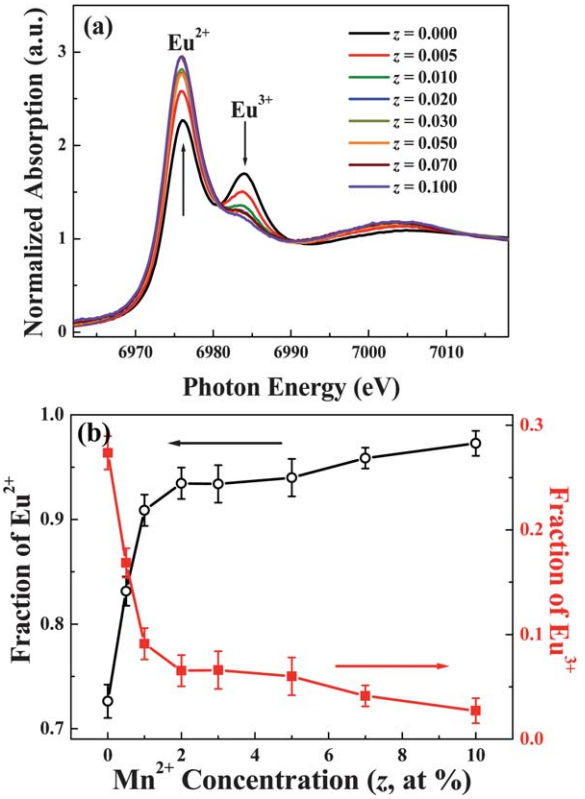

Fig. 6 (a) Eu L_3-edge XANES spectra of CSYP:0.007Eu^{2+},zMn^{2+} phosphor. (b) Fraction of Eu^{2+} as a function of Mn^{2+} concentration.

opposite trend to the increased Mn^{2+} concentration (as shown in Fig. 5b), an energy transfer from Eu^{2+} to Mn^{2+} *via* a non-radiative process was thought to occur owing to the overlap between the Eu^{2+} emission and the Mn^{2+} excitation spectra. For $z < 0.01$, the PL behavior of Eu^{2+} can be attributed to the competing effects of the increased Eu^{2+} ions and the energy transfer, where the latter is dominated. As Mn^{2+} content increases further ($z > 0.01$), the variations in emission spectra of Eu^{2+} and Mn^{2+} are contributed from both the energy transfer and the Mn^{2+} concentration effects.

3.3 Luminescent decay times

The decay process of CSYP:0.007Eu^{2+},zMn^{2+} phosphors was also investigated and shown in Fig. 7. The corresponding luminescent decay times can be fitted well with a second-order exponential decay curve by the following equation:[21,22]

$$I = A_1\exp(-t/\tau_1) + A_2\exp(-t/\tau_2) \quad (2)$$

where I is the luminescence intensity; A_1 and A_2 are constants; t is the time; and τ_1 and τ_2 are respectively short and long lifetimes for exponential components. Using these parameters, the average decay time (τ^*) can be determined by the formula as follows:[23]

$$\tau^* = (A_1\tau_1^2 + A_2\tau_2^2)/(A_1\tau_1 + A_2\tau_2) \quad (3)$$

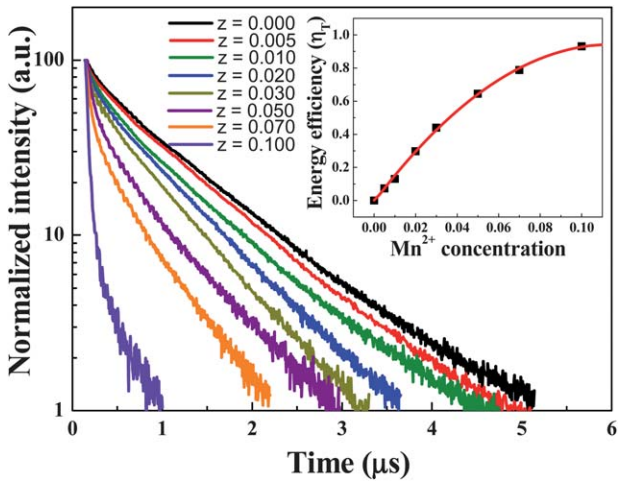

Fig. 7 Decay curves of Eu^{2+} emission for CSYP:0.007Eu^{2+},zMn^{2+} phosphors under excitation at 380 nm, monitored at 508 nm. The inset shows the relation of η_T *versus* Mn^{2+} ion concentration.

The values of τ_1, A_1, τ_2, and A_2 are analyzed and listed in Table 3. The average decay times (τ*) were calculated to be 993, 920, 863, 697, 556, 353, 211 and 68.9 ns for CSYP:0.007Eu^{2+},zMn^{2+} with $z = 0$, 0.005, 0.01, 0.02, 0.03, 0.05, 0.07, and 0.1, respectively. Furthermore, the energy transfer efficiency (η_T) from the sensitizer Eu^{2+} to the activator Mn^{2+} can be calculated by:[24]

$$\eta_T = 1 - \frac{\tau_S}{\tau_{S0}} \quad (4)$$

where τ_{S0} and τ_S are respectively the lifetime of Eu^{2+} in the absence and presence of Mn^{2+}. The energy transfer efficiency from a sensitizer Eu^{2+} to an activator Mn^{2+} in CSYP was plotted as a function of z in the inset of Fig. 7.

More precisely, the η_T was determined to be 0%, 7.35%, 13.1%, 29.8%, 44%, 64.5%, 78.8% and 93.1% for CSYP:0.007Eu^{2+},zMn^{2+} with $z = 0$, 0.005, 0.01, 0.02, 0.03, 0.05, 0.07, and 0.1, respectively. These results indicate that the η_T increases monotonically with increasing doped Mn^{2+} concentration.

3.4 Energy transfer mechanism and critical distance

The energy transfer mechanism for exchange/multipolar interactions has been discussed by many authors[25–27] and can be expressed by:

Table 3 Decay times of $(Ca_{0.493-z}Sr_{0.5})_9Y(PO_4)_7$:0.007$Eu^{2+}$,z$Mn^{2+}$ phosphors with emission monitored at 508 nm

Sample	τ_1	A_1	τ_2	A_2	τ* (ns)
$z = 0.000$	1.96E-07	52.25	1.08E-06	86.58	993
$z = 0.005$	1.79E-07	58.15	1.01E-06	85.33	920
$z = 0.010$	1.53E-07	73.79	9.63E-07	82.94	863
$z = 0.020$	1.02E-07	118.43	8.09E-07	79.32	697
$z = 0.030$	7.32E-08	219.34	7.06E-07	73.15	556
$z = 0.050$	6.86E-08	566.12	6.48E-07	57.74	353
$z = 0.070$	6.19E-08	877.43	5.24E-07	49.24	211
$z = 0.100$	2.93E-08	1162.92	2.77E-07	23.43	68.9

$$\ln\frac{\tau_{S0}}{\tau_S} \propto C \quad \text{and} \quad \frac{\tau_{S0}}{\tau_S} \propto C^{\alpha/3} \quad (5)$$

where C is the concentration of Mn^{2+}. The relation of $\ln(\tau_{S0}/\tau_S) \propto C$ corresponds to the exchange interaction, while the relations of $(\tau_{S0}/\tau_S) \propto C^{\alpha/3}$ with $\alpha = 6$ and 8 correspond to dipole–dipole and dipole–quadrupole interactions, respectively. Fig. 8 presents the plots of $\ln(\tau_{S0}/\tau_S)$ *versus* C as well as (τ_{S0}/τ_S) *versus* $C^{\alpha/3}$. A linear relation is obtained only when $\alpha = 8$; therefore, the energy absorbed by Eu^{2+} is transferred to Mn^{2+} *via* a non-radiative dipole–quadrupole mechanism. The above results indicate that energy transfer occurs from a sensitizer Eu^{2+} to an activator Mn^{2+} in the CSYP:0.007Eu^{2+},zMn^{2+} phosphor and that emission intensity and CIE chromaticity coordinates could be tuned by different concentration ratios of Eu^{2+}/Mn^{2+}.

According to a dipole–quadrupole mechanism, the critical distance of energy transfer from Eu^{2+} to Mn^{2+} can be expressed by:[28]

$$W_{sa}^{DQ} = \frac{3\hbar^4 c^4 f_q \lambda_s^2 Q_a}{4\pi n^4 \tau_s^0 f_d R_{sa}^8} \Omega(F_s, F_a) \quad (6)$$

where $\hbar$, c, π, and n are constants; τ_s^0 is the intrinsic lifetime of the sensitizer; $f_d = 10^{-7}$ and $f_q = 10^{-10}$ are the respective oscillator strengths of the activator dipole and quadrupole transitions; λ_s (in Å) is the emission wavelength of the sensitizer Eu^{2+}; $Q_a = 4.8 \times 10^{-16}$ is the integrated absorption coefficient of the acceptor Mn^{2+}; R_{sa} is the distance between the ions involved in the transfer; and $\Omega(F_s,F_a) = \int F_s(E)F_a(E)E^{-4}dE$ represents the spectral overlap between the Eu^{2+} emission $F_s(E)$ and the Mn^{2+} absorption $F_a(E)$, which was estimated to be about 2.94×10^{-2} eV^{-5}. The critical distance of energy transfer from Eu^{2+} to Mn^{2+} is defined as the distance at which the energy transfer rate is equal to the intrinsic rate of the sensitizer, *i.e.*, $W_{sa}^{DQ}\tau_s^0 = 1$. Therefore, the critical distance for a dipole–quadrupole type energy transfer was calculated to be 11.09 Å, in fairly good agreement to those values reported in the literature.[26,27]

3.5 CIE color coordinates and LED lamp fabrication

The CIE chromaticity diagram of CYP:0.007Eu^{2+},xMg^{2+}, CYP:0.007Eu^{2+},ySr^{2+}, and CSYP:0.007Eu^{2+},zMn^{2+} phosphors

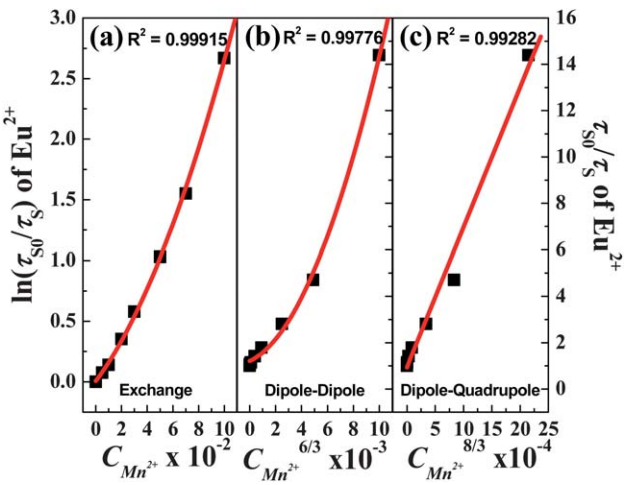

Fig. 8 Dependence of (a) $\ln(\tau_{S0}/\tau_S)$ of Eu^{2+} on C_{Mn}^{2+}, and that of τ_{S0}/τ_S of Eu^{2+} on (b) $C_{Mn^{2+}}^{6/3}$, (c) $C_{Mn^{2+}}^{8/3}$.

under 380 nm excitation is shown in Fig. 9. The color tone can be tuned from blue-greenish (0.179, 0.301) to blue (0.162, 0.098) and from blue-greenish (0.179, 0.301) to green (0.273, 0.459), respectively, by doping various concentrations of Mg^{2+} (x = 0.05–0.5) and Sr^{2+} (y = 0.05–0.5). The shift through the CIE chromaticity diagram with different Eu^{2+}/Mn^{2+} ratios in CSYP:0.007Eu^{2+},zMn^{2+} (z = 0–0.1) phosphors is from green (0.273, 0.459) through yellow (0.358, 0.431) and eventually to red (0.565, 0.360).

Fig. 10 shows the electroluminescence (EL) spectrum of a white-light LED fabricated using a 380 nm n-UV LED chip combined with yellow-emitting CSYP:0.007Eu^{2+},0.02Mn^{2+} (0.358, 0.431) and blue-emitting CMYP:0.007Eu^{2+} (0.162, 0.098) phosphors and driven by a 350 mA current.

The EL spectrum clearly shows four emission bands at 380, 435, 508, and 632 nm, which arise respectively from the n-UV chip, CMYP:0.007Eu^{2+}, and CSYP:0.007Eu^{2+},0.02Mn^{2+} phosphors. The optical properties of the white-light LED show a correlated color temperature (CCT) of 6303 K, a color-rendering index (CRI) of 87.4, and CIE color coordinates x = 0.314 and y = 0.348. The 14 CRIs and the average color-rendering index Ra = 87.4 are given in Table 4. The inset of Fig. 9 shows external views of a white-light LED lamp and of a white-emitting n-UV LED driven by a 350 mA current. These results indicate that the CRI of white light generated by a combination of CSYP:0.007Eu^{2+},0.02Mn^{2+} and CMYP:0.007Eu^{2+} phosphors was higher than that produced by YAG:Ce^{3+} (Ra = 75)[3] since the former contains all the red, green, and blue light components. Therefore, a mixture of CSYP:0.007Eu^{2+},0.02Mn^{2+} and CMYP:0.007Eu^{2+} phosphors may have promising applications for white-light near-UV LEDs.

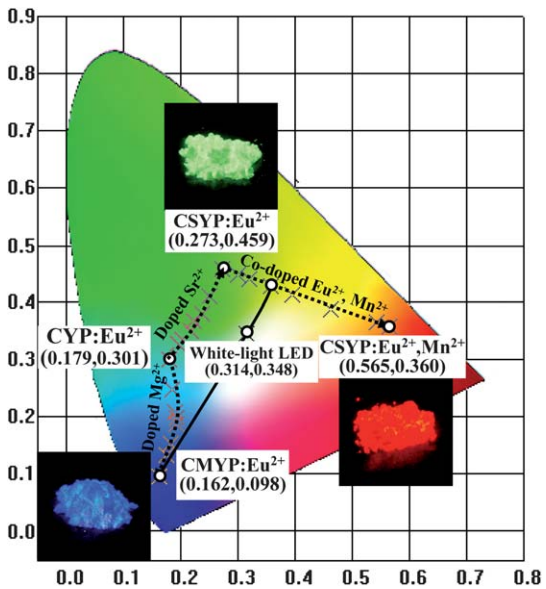

Fig. 9 CIE chromaticity diagram of CYP:0.007Eu^{2+},xMg^{2+} (x = 0.05–0.5), CYP:0.007Eu^{2+},ySr^{2+} (y = 0.05–0.5), and CSYP:0.007Eu^{2+},zMn^{2+} (z = 0–0.1) phosphors under 380 nm excitation.

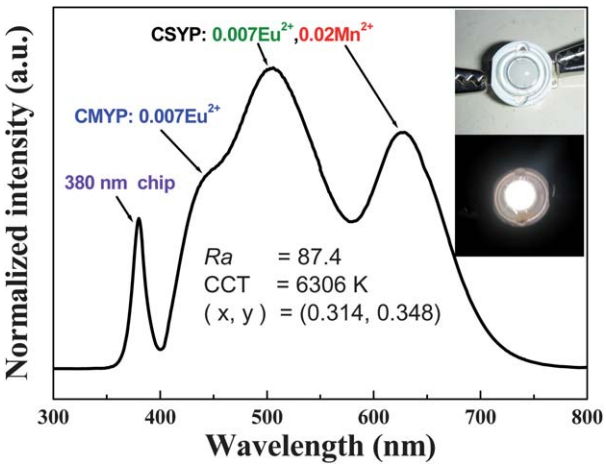

Fig. 10 EL spectrum of a white-emitting LED using a 380 nm n-UV chip comprising CSYP:0.007Eu^{2+},0.02Mn^{2+} (yellow) and CMYP:0.007Eu^{2+} (blue) phosphors driven by a 350 mA current.

Table 4 Full set of 14 CRIs and Ra of CSYP:0.007Eu^{2+},0.02Mn^{2+} and CMYP:0.007Eu^{2+} phosphor with 380 nm n-UV chip

R_1	R_2	R_3	R_4	R_5	R_6	R_7	R_8	R_9	R_{10}	R_{11}	R_{12}	R_{13}	R_{14}	Ra
85	91	92	86	87	86	90	82	50	76	81	84	86	95	87.4

4 Conclusions

In summary, we have demonstrated the synthesis of two series of novel $(Ca,Mg,Sr)_9Y(PO_4)_7$:Eu^{2+} and $(Ca_{0.5}Sr_{0.5})_9Y(PO_4)_7$: Eu^{2+}, Mn^{2+} phosphors *via* high-temperature solid-state reactions. Their emission color was tunable through crystal field splitting and energy transfer. Crystal field splitting (Dq) of the $Ca_9Y(PO_4)_7$:0.07Eu^{2+} host decreased when Ca^{2+} was substituted by a smaller Mg^{2+} ion and increased when Ca^{2+} was substituted by a larger Sr^{2+} ion. Energy transfer from the sensitizer Eu^{2+} to the activator Mn^{2+} in $(Ca_{0.5}Sr_{0.5})_9Y(PO_4)_7$:$Eu^{2+}$,$Mn^{2+}$ phosphors was found to be an electric dipole–quadrupole interaction. The critical distance was calculated to be 11.09 Å. Moreover, a trichromatic white LED, fabricated by integrating a 380 nm n-UV chip, yellow-emitting CSYP:0.007Eu^{2+},0.02Mn^{2+}, and blue-emitting CMYP:0.007Eu^{2+} phosphors into a single package, shows a white light with a CCT of 6303 K, Ra of 87.4, and CIE of (0.314, 0.348). These results indicate that a near-UV chip coupled with CSYP:0.007Eu^{2+},0.02Mn^{2+} and CMYP:0.007Eu^{2+} phosphors can effectively enhance the CRIs as compared to those of blue-chips combined with a YAG:Ce^{3+}-based white LED.

Acknowledgements

This research was supported by National Science Council of Taiwan, R.O.C. under contract No. NSC98-2113-M-009-005-MY3 (T.-M. C.). One of the authors (P. J. Wu) thanks Chih-Wen Pao for assistance in the XANES experiments.

References

1 V. Bachmann, C. Ronda and A. Meijerink, *Chem. Mater.*, 2009, **21**, 2077.

2 K. Zhang, W. B. Hu, Y. T. Wu and H. Z. Liu, *Inorg. Mater.*, 2008, **44**, 1218.
3 H. S. Jang, Y. H. Won and D. Y. Jeon, *Appl. Phys. B: Lasers Opt.*, 2009, **95**, 715.
4 A. A. Setlur, W. J. Heward, Y. Gao, A. M. Srivastava, R. G. Chandran and M. V. Shankar, *Chem. Mater.*, 2006, **18**, 3314.
5 M. Batentschuk, A. Osvet, G. Schierning, A. Klier, J. Schneider and A. Winnacker, *Radiat. Meas.*, 2004, **38**, 539.
6 Y. C. Chiu, W. R. Liu, C. K. Chang, C. C. Liao, Y. T. Yeh, S. M. Jang and T. M. Chen, *J. Mater. Chem.*, 2010, **20**, 1755.
7 C. Guo, L. Luan, Y. Xu, F. Gao and L. Liang, *J. Electrochem. Soc.*, 2008, **155**, J310.
8 S. H. Lee, J. H. Park, S. M. Son and J. S. Kim, *Appl. Phys. Lett.*, 2006, **89**, 221916.
9 JCPDS file no. 046–0402.
10 C. Zhang, J. Yang, C. Lin, C. Li and J. Lin, *J. Solid State Chem.*, 2009, **182**(7), 1673.
11 J. M. Robertson, M. W. van Tol, W. H. Smits and J. P. H. Heyene, *Philips J. Res.*, 1981, **36**, 15.
12 H. S. Jang, W. B. Im, D. C. Lee, D. Y. Jeon and S. S. Kim, *J. Lumin.*, 2007, **126**, 371.
13 P. D. Rack and P. H. Holloway, *Mater. Sci. Eng., R*, 1998, **21**, 171.
14 P. Y. Jia, J. Lin, X. M. Han and M. Yu, *Thin Solid Films*, 2005, **483**, 122.
15 R. V. S. S. N. Ravikumar, K. Ikeda, A. V. Chandrasekhar, Y. P. Reddy, P. S. Rao and J. Yamauchi, *J. Phys. Chem. Solids*, 2003, **64**, 2433.
16 C. Guo, L. Luan, X. Ding and D. Huang, *Appl. Phys. A: Mater. Sci. Process.*, 2008, **91**, 327.
17 Z. Qi, C. Shi, M. Liu, D. Zhou, X. Luo, J. Zhang and Y. Xie, *Phys. Status Solidi A*, 2004, **201**, 3109.
18 K. S. Sohn, S. S. Kim and H. D. Park, *Appl. Phys. Lett.*, 2002, **81**, 1759.
19 T. G. Kim, H. S. Lee, C. C. Lin, T. Kim, R. S. Liu, T. S. Chan and S. J. Im, *Appl. Phys. Lett.*, 2010, **96**, 061904.
20 J. Petiau, G. Calas, D. Petitmaire, A. Bianconi, M. Benfatto and A. Marcelli, *Phys. Rev. B*, 1986, **34**, 7350.
21 W. Y. Shen, M. L. Pang, J. Lin and J. Fang, *J. Electrochem. Soc.*, 2005, **152**(2), H25.
22 M. Yu, J. Lin and J. Fang, *Chem. Mater.*, 2005, **17**(7), 1783.
23 N. Ruelle, M. P. Thi and C. Fouassier, *Jpn. J. Appl. Phys.*, 1992, **31** (Part 1, No. 9A), 2786.
24 C. H. Huang and T. M. Chen, *Opt. Express*, 2010, **18**, 5089.
25 C. H. Huang, W. R. Liu and T. M. Chen, *J. Phys. Chem. C*, 2010, **114**, 18698.
26 C. K. Chang and T. M. Chen, *Appl. Phys. Lett.*, 2007, **90**, 161901.
27 W. J. Yang, L. Luo, T. M. Chen and N. S. Wang, *Chem. Mater.*, 2005, **17**, 3883.
28 C. H. Huang, T. M. Chen, W. R. Liu, Y. C. Chiu, Y. T. Yeh and S. M. Jang, *ACS Appl. Mater. Interfaces*, 2010, **2**, 259.